Int. J. Electron. Commun. (AEÜ) 127 (2020) 153447

Contents lists available at ScienceDirect

Int. J. Electron. Commun. (AEÜ)

journal homepage: www.elsevier.com/locate/aeue

Regular paper

Fringing field correction for spherical–rectangular microstrip antennas

Camila Almeida Diniz [a], Leonardo Aquino Costa [b], Odilon Maroja da Costa Pereira-Filho [c,*], Fernando Jose da Silva Moreira [d]

[a] Instituto Federal de Pernambuco, Afogados da Ingazeira, Brazil
[b] PETROBRAS, Rio de Janeiro, Brazil
[c] Universidade Federal de Pernambuco, Centro de Informatica, Recife, Brazil
[d] Universidade Federal de Minas Gerais, Departamento de Eletronica, Belo Horizonte, Brazil

ARTICLE INFO

Keywords:
Microstrip antennas
Spherical antennas
Conformal antennas
Spherical patches

ABSTRACT

This paper presents the analysis of spherical–rectangular patches using both cavity method and method of moments. A detailed procedure of cavity method is presented, including the field distribution inside the cavity, equivalent magnetic current distributions, radiation fields, effective loss tangent, and input impedance. A new fringing field correction is proposed taking into account the curvature of the patch, resulting in accurate resonance frequency.

1. Introduction

Microstrip antennas have been widely used due to their low cost, electrical properties, as well as their ability to connect to microwave circuits. In many applications the microstrip antennas need to adjust to non planar surfaces, as in satellites, rockets, airplanes, or for wearable antennas. These conformal geometries, like cylindrical [1,2], spherical [3,4] or conical [5,6], also allow different radiation and electrical properties, and are used accordingly. Spherical microstrip antennas are those printed onto a spherically shaped dielectric layer that covers a spherical conductor. Usual shapes of the spherical antennas include the circular, annular-ring, and rectangular (or quasi-rectangular) patches.

Nonplanar microstrip antennas have been described, for different antenna shapes, arrays, and analysis methods [7,8]. Particularly, spherical microstrip antennas have been studied using several techniques, including cavity method [9–14], electric surface current method [15], Generalized Transmission Line Model (GTLM) [16,17], and Method of Moments (MoM) [18–26]. Although cavity method is among the simplest ones, it provides invaluable physical insight about the field distribution and current excitation on the patch. It assumes the fields in the dielectric to be bounded in the volume between the antenna and the spherical conductor, where they are determined from expansion in cavity eigenmodes. Radiation properties are obtained from equivalent magnetic surface currents on the cavity side walls, neglecting the presence of the dielectric layer. Despite its simplicity the method results in accurate radiation patterns. Additionally, evaluation of input impedances requires the determination of equivalent loss tangent, including dielectric, radiation and conductor losses, and a correction on the resonant length of the antenna is required to account for fringe fields. Previous contributions using cavity method for spherical microstrip antenna include obtaining the radiation efficiency [9] and radiation patterns [10] for spherical–rectangular microstrip antennas, and for circular disk and annular ring [11–13]. In [14] a Mathematica based CAD was presented using cavity method to obtain input impedances and radiation patterns of spherical annular and circular microstrip antennas. On the other hand, the electric surface current method assumes the electric current on the surfaces of the patches to be known, either from cavity method or any other source, and computes the radiation fields and input impedance using the proper Green's functions, including the presence of the dielectric layer. It was used in [15] for determining the radiation patterns of microstrip spherical circular disk antennas. The input impedance can also be obtained from GTLM, by modeling the antenna as a transmission line loaded with wall admittances, as in [16] for spherical circular, and in [17] for spherical annular antennas. The MoM is a full-wave method in which the electric current distribution on the patches are expanded into a set of known functions. The expansion coefficients are determined by imposing the boundary conditions on the patch surface. Appropriate symmetric products by a set of weighting functions transform the boundary condition equations into a linear system, from which the expansion coefficients are determined. MoM was used in [19–21] to obtain resonances, radiation patterns, and input impedances of spherical circular and annular microstrip antennas. It was also used in [22–25]

* Corresponding author.
E-mail addresses: camilla.a.diniz@gmail.com (C.A. Diniz), leonardoaquino@yahoo.com.br (L.A. Costa), odilon@cin.ufpe.br (O.M.d.C. Pereira-Filho), fernandomoreira@ufmg.br (F.J.d.S. Moreira).

https://doi.org/10.1016/j.aeue.2020.153447
Received 5 March 2019; Accepted 31 August 2020
Available online 7 September 2020

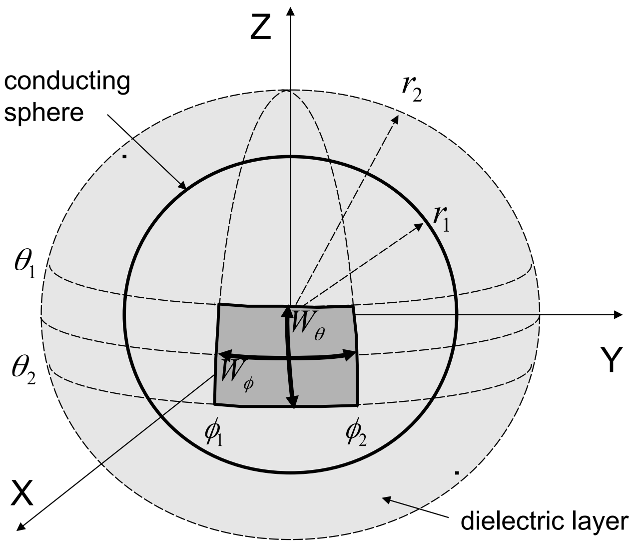

Fig. 1. Geometry of the spherical–rectangular microstrip patch.

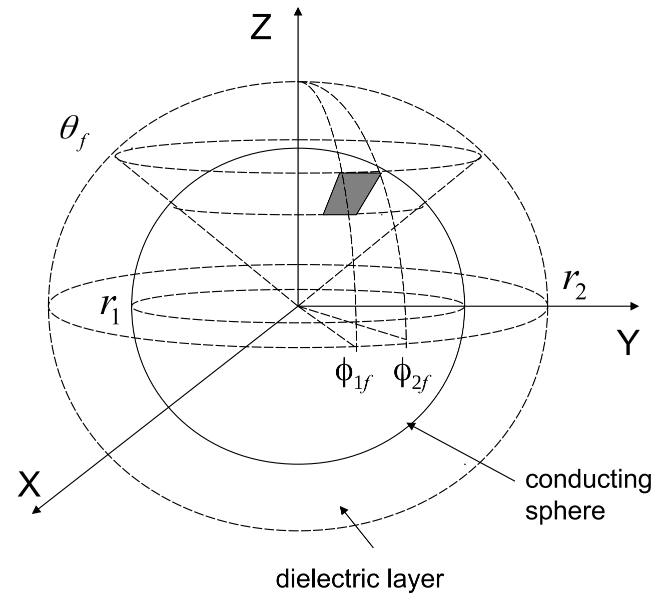

Fig. 2. Feeding strip representing the coaxial cable.

to analyze spherical–rectangular microstrip antennas and arrays, and in [26,27] to analyze spherical–trapezoidal microstrip antennas and arrays. Procedures for evaluation of Green's functions in spherically layered media were presented in [28–30]. And results for circular and quasi-rectangular microstrip antennas for multilayered spherical media were shown in [31,32]. Curvilinear Rao–Wilton–Glisson triangular basis functions were used in [33,34] for modeling antennas in spherically layered media.

This paper presents the application of cavity method to spherical–rectangular patches, and introduces a new fringing field correction to take into account the patch curvature. Section 2 describes the geometry of the spherical microstrip patches. Section 3 shows the application of cavity method to these antennas. Section 4 describes the application of MoM to spherical microstrip antennas. Section 5 describes how the fringing field corrections used for planar microstrip antennas can be modified to account for the curvature of spherical patches. Results are presented in Section 6 comparing the solutions.

2. Geometry of the antennas

Fig. 1 shows the geometry of the spherical–rectangular microstrip patch. A metallic sphere of radius r_1 is covered by a dielectric layer of thickness h ($r_2 = r_1 + h$), relative permittivity ε_r, and loss tangent $\tan\delta_d$. The patch is printed onto the dielectric surface at $r = r_2$, limited by angles θ_1, θ_2, ϕ_1, and ϕ_2, in spherical coordinates. And fed by coaxial cables centered at θ_f and ϕ_f. For simplicity the inner conductor of the coaxial cable feeding the patch is modeled as a strip [35] at θ_f, $r_1 < r < r_2$, and $\phi_{1f} < \phi < \phi_{2f}$, as presented in Fig. 2.

3. Application of cavity method

The cavity method assumes the fields in the dielectric layer to be confined within the region below the patch, i.e., in a cavity formed by the patch, the metallic sphere, and perfect magnetic conductors on the side walls [9–14].

3.1. Cavity fields

Usually the thickness of the dielectric layer is small compared to the wavelength, and the fields in the cavity are almost independent of r. Assuming no radial variation ($\partial/\partial r = 0$), only TM^r fields are excited in the cavity, and the radial electric field is the solution of:

$$\frac{1}{r_{12}^2 \sin\theta}\frac{\partial}{\partial\theta}\left(\sin\theta\,\frac{\partial E_r}{\partial\theta}\right) + \frac{1}{r_{12}^2\sin^2\theta}\frac{\partial^2 E_r}{\partial\phi^2} + k_d^2 E_r = j\omega\mu J_f \tag{1}$$

where $r_{12} = (r_1 + r_2)/2$, $k_d = \omega\sqrt{\mu\varepsilon_d}$ is the wave number in the dielectric, $\varepsilon_d = \varepsilon_o\varepsilon_r\left(1 - j\tan\delta_d\right)$ is the complex permittivity of the dielectric, and J_f is the volume density of the feed current in radial direction. The electric field in the cavity can be expanded into TM^r modes, already satisfying the boundary conditions on the patch, metallic sphere and perfect magnetic walls:

$$E_r(\theta,\phi) = \sum_u \sum_l e_{lu}\, E_{r,lu}(\theta,\phi) \tag{2}$$

where e_{lu} are the coefficients of the expansion, and the eigenmodes $E_{r,lu}$ are solution of the source-free problem:

$$\frac{1}{r_{12}^2 \sin\theta}\frac{\partial}{\partial\theta}\left(\sin\theta\,\frac{\partial E_{r,lu}}{\partial\theta}\right) + \frac{1}{r_{12}^2\sin^2\theta}\frac{\partial^2 E_{r,lu}}{\partial\phi^2} + k_{lu}^2 E_{r,lu} = 0 \tag{3}$$

These modes are obtained by imposing the boundary conditions on the cavity walls $\theta = \theta_1$, $\phi = \phi_1$, $\phi = \phi_2$, and are given by:

$$E_{r,lu} = \left[P_l^u(\cos\theta)\frac{d}{d\theta}Q_l^u(\cos\theta_1) - \frac{d}{d\theta}P_l^u(\cos\theta_1)Q_l^u(\cos\theta)\right]\cos\left(u(\phi-\phi_1)\right) \tag{4}$$

where $P_l^u(\cdot)$ and $Q_l^u(\cdot)$ are associated Legendre functions, $u = \frac{p\pi}{\Delta\phi}$, $p = 0, 1, 2, \ldots$, and $\Delta\phi = \phi_2 - \phi_1$. The values of eigenvalue l, for a given u, are obtained from the transcendental equation below, that ensures the boundary condition on the side wall $\theta = \theta_2$:

$$\frac{d}{d\theta}P_l^u(\cos\theta_2)\frac{d}{d\theta}Q_l^u(\cos\theta_1) - \frac{d}{d\theta}P_l^u(\cos\theta_1)\frac{d}{d\theta}Q_l^u(\cos\theta_2) = 0 \tag{5}$$

and

$$k_{lu} = \frac{\sqrt{l(l+1)}}{r_{12}} \tag{6}$$

While the modal electric field has only r-component (4), the magnetic field has θ and ϕ-components given by [36]:

$$H_{\theta,lu} = \frac{-1}{jw\mu r_{12}\sin\theta}\frac{\partial E_{r,lu}}{\partial\phi} = \frac{u}{jw\mu\, r_{12}\sin\theta}\left[P_l^u(\cos\theta)\frac{d}{d\theta}Q_l^u(\cos\theta_1) - \frac{d}{d\theta}P_l^u(\cos\theta_1)Q_l^u(\cos\theta)\right] \times \sin\left(u(\phi-\phi_1)\right) \quad (7)$$

$$H_{\phi,lu} = \frac{1}{jw\mu r_{12}}\frac{\partial E_{r,lu}}{\partial\theta} = \frac{1}{jw\mu\, r_{12}}\left[\frac{d}{d\theta}P_l^u(\cos\theta)\frac{d}{d\theta}Q_l^u(\cos\theta_1) - \frac{d}{d\theta}P_l^u(\cos\theta_1)\frac{d}{d\theta}Q_l^u(\cos\theta)\right] \times \cos\left(u(\phi-\phi_1)\right) \quad (8)$$

Assuming the feed current to be uniform across the strip, see Fig. 2, its volume distribution, corresponding to a total current I_o, is given by:

$$J_f(r,\theta,\phi) = \frac{I_o}{r_{12}^2\sin(\theta_f)\Delta\phi_f}\delta(\theta-\theta_f) \quad (9)$$

for $r_1 < r < r_2$ and $\phi_{1f} < \phi < \phi_{2f}$, where $\Delta\phi_f = \phi_{2f} - \phi_{1f}$. Substituting the eigenmode expansion (2) in (1) and using (4):

$$\sum_u\sum_l e_{lu}\left(k_d^2 - k_{lu}^2\right)E_{r,lu}(\theta,\phi) = jw\mu J_f \quad (10)$$

Using the orthogonality of the eigenmodes $E_{r,lu}$, the expansion coefficients e_{lu} are given by:

$$e_{lu} = \frac{jw\mu}{k_d^2 - k_{lu}^2}\frac{\langle J_f, E_{r,lu}\rangle}{\|E_{r,lu}\|^2} \quad (11)$$

where the inner product is defined as:

$$\langle f,g\rangle = \int_0^\pi\int_{-\pi}^\pi f(\theta,\phi)g^*(\theta,\phi)\sin\theta\, d\phi\, d\theta \quad (12)$$

Substituting the expansion coefficients e_{lu} (11) in (2), the electric field in the cavity is given by:

$$E_r(\theta,\phi) = \sum_u\sum_l \frac{jw\mu}{k_d^2 - k_{lu}^2}\frac{\langle J_f, E_{r,lu}\rangle}{\|E_{r,lu}\|^2}E_{r,lu}(\theta,\phi) \quad (13)$$

where the inner product $\langle J_f, E_{r,lu}\rangle$ is given by:

$$\langle J_f, E_{r,lu}\rangle = \frac{I_o}{r_{12}^2}\left[P_l^u(\cos\theta_f)\frac{d}{d\theta}Q_l^u(\cos\theta_1) - \frac{d}{d\theta}P_l^u(\cos\theta_1)Q_l^u(\cos\theta_f)\right]\times \operatorname{sinc}\left(\frac{u\Delta\phi_f}{2\pi}\right)\cos\left(u(\phi_f-\phi_1)\right) \quad (14)$$

where $\operatorname{sinc}(x) = \sin(\pi x)/(\pi x)$. And the squared norm of $E_{r,lu}$ is given by:

$$\|E_{r,lu}\|^2 = \frac{\Delta\phi}{\tau_u}\int_{\theta_1}^{\theta_2}\left[P_l^u(\cos\theta)\frac{d}{d\theta}Q_l^u(\cos\theta_1) - \frac{d}{d\theta}P_l^u(\cos\theta_1)Q_l^u(\cos\theta)\right]^2 \times \sin\theta\, d\theta \quad (15)$$

where $\tau_u = 1$ if $u = 0$, and $\tau_u = 2$ if $u \neq 0$.

3.2. External fields

The fields external to the cavity can be obtained with the aid of the equivalence principle [36]. Equivalent magnetic current surface densities are obtained from the electric fields at the four side walls of the cavity. Due to the small thickness of the dielectric, these surface current densities can be concentrated as surface current distributions on the metallic sphere ($r = r_1$):

$$\bar{M}_{s1}(\theta,\phi) = -E_r(\theta_1,\phi)\frac{h}{r_1}\delta(\theta-\theta_1)\hat{a}_\phi \qquad \phi_1<\phi<\phi_2 \quad (16)$$

$$\bar{M}_{s2}(\theta,\phi) = E_r(\theta_2,\phi)\frac{h}{r_1}\delta(\theta-\theta_2)\hat{a}_\phi \qquad \phi_1<\phi<\phi_2 \quad (17)$$

$$\bar{M}_{s3}(\theta,\phi) = E_r(\theta,\phi_1)\frac{h}{r_1\sin\theta}\delta(\phi-\phi_1)\hat{a}_\theta \qquad \theta_1<\theta<\theta_2 \quad (18)$$

$$\bar{M}_{s4}(\theta,\phi) = -E_r(\theta,\phi_2)\frac{h}{r_1\sin\theta}\delta(\phi-\phi_2)\hat{a}_\theta \qquad \theta_1<\theta<\theta_2 \quad (19)$$

The external fields generated by the magnetic sources (16)–(19), ignoring the presence of the dielectric layer, can be obtained using field expansion in TM_{mn}^r and TE_{mn}^r external modes, obtained using the vector potentials:

$$A_r^o(r,\theta,\phi) = \sum_{n=1}^\infty\sum_{m=-n}^n e_{nm}\hat{H}_n^{(2)}(k_o\, r)\bar{P}_n^{|m|}(\cos\theta)e^{jm\phi} \quad (20)$$

$$F_r^o(r,\theta,\phi) = \sum_{n=1}^\infty\sum_{m=-n}^n f_{nm}\hat{H}_n^{(2)}(k_o\, r)\bar{P}_n^{|m|}(\cos\theta)e^{jm\phi} \quad (21)$$

where $\hat{H}_n^{(2)}(.)$ is the Schelkunoff Hankel function of second kind, $\bar{P}_n^{|m|}(.)$ is the normalized associated Legendre function, as defined in (78), superscript $\}\}o''$ in A_r^o and F_r^o stands for free space, and $k_o = w\sqrt{\mu\varepsilon_o}$ is the wave number in free space. The electric field can be obtained from the vector potentials [36]:

$$E_r = \frac{1}{jw\varepsilon}\left(\frac{\partial^2}{\partial r^2} + k^2\right)A_r \quad (22)$$

$$E_\theta = \frac{-1}{r\sin\theta}\frac{\partial F_r}{\partial\phi} + \frac{1}{jw\varepsilon\, r}\frac{\partial^2 A_r}{\partial r\,\partial\theta} \quad (23)$$

$$E_\phi = \frac{1}{r}\frac{\partial F_r}{\partial\theta} + \frac{1}{jw\varepsilon\, r\sin\theta}\frac{\partial^2 A_r}{\partial r\,\partial\phi} \quad (24)$$

$$H_r = \frac{1}{jw\mu}\left(\frac{\partial^2}{\partial r^2} + k^2\right)F_r \quad (25)$$

$$H_\theta = \frac{1}{r\sin\theta}\frac{\partial A_r}{\partial\phi} + \frac{1}{jw\mu\, r}\frac{\partial^2 F_r}{\partial r\,\partial\theta} \quad (26)$$

$$H_\phi = \frac{-1}{r}\frac{\partial A_r}{\partial\theta} + \frac{1}{jw\mu\, r\sin\theta}\frac{\partial^2 F_r}{\partial r\,\partial\phi} \quad (27)$$

The radiated power associated to each external mn-mode (of unitary amplitude) is given by:

$$P_{r,mn} = \frac{1}{2}\int_0^\pi\int_0^{2\pi}\Re\left[\bar{E}_{mn}\times\bar{H}_{mn}^*\right]\cdot\hat{a}_r\, r^2\sin\theta\, d\phi\, d\theta \quad (28)$$

which results in:

$$P_{r,mn}^{TM} = \frac{\eta_o}{2}S(n) \quad (29)$$

$$P_{r,mn}^{TE} = \frac{1}{2\eta_o}S(n) \quad (30)$$

where $\eta_o = \sqrt{\mu/\varepsilon_o}$ is the intrinsic impedance of free space and $S(n)$ is given by (77).

In the normalized vector Legendre domain, see Appendix:

$$\tilde{E}^o(r,n,m) = \begin{bmatrix}E_u^o(r,n,m)\\ E_d^o(r,n,m)\end{bmatrix} = \begin{bmatrix}-j\eta_o\sqrt{S(n)}\hat{H}_n^{(2)\prime}(k_o r)\, e_{nm}/r\\ \sqrt{S(n)}\hat{H}_n^{(2)}(k_o r)\, f_{nm}/r\end{bmatrix} \quad (31)$$

$$\tilde{H}^o(r,n,m) = \begin{bmatrix}H_u^o(r,n,m)\\ H_d^o(r,n,m)\end{bmatrix} = \begin{bmatrix}-j\sqrt{S(n)}\hat{H}_n^{(2)\prime}(k_o r)\, f_{nm}/(\eta_o r)\\ -\sqrt{S(n)}\hat{H}_n^{(2)}(k_o r)\, e_{nm}/r\end{bmatrix} \quad (32)$$

The coefficients e_{nm} and f_{nm} are determined from the boundary conditions at $r = r_1$ interface:

$$\bar{M}_s(\theta,\phi) = -\hat{a}_r\times\bar{E}(r_1,\theta,\phi) \quad (33)$$

which can also be written in the normalized vector Legendre domain, as:

$$\begin{bmatrix}M_u(n,m)\\ M_d(n,m)\end{bmatrix} = \begin{bmatrix}0 & 1\\ -1 & 0\end{bmatrix}\begin{bmatrix}E_u(r_1,n,m)\\ E_d(r_1,n,m)\end{bmatrix} \quad (34)$$

Substituting (31) into (34), the coefficients e_{nm} and f_{nm} are given by:

$$e_{nm} = \frac{r_1}{j\eta_o\sqrt{S(n)}\hat{H}_n^{(2)\prime}(k_o r_1)}M_d(n,m) \quad (35)$$

$$f_{nm} = \frac{r_1}{\sqrt{S(n)}\hat{H}_n^{(2)}(k_o r_1)}M_u(n,m) \quad (36)$$

where $M_u(n,m)$ and $M_d(n,m)$ are obtained from substituting (16)–(19) into (75).

3.3. Input impedance

The input impedance at the probe is given by the variational expression [36]:

$$Z_{in} = -\frac{1}{I_o^2}\iint_S \bar{E}(\bar{J}_f)\cdot \bar{J}_f\,ds \tag{37}$$

Substituting (9) and (13) results:

$$Z_{in} = -\frac{h}{I_o^2}\sum_u\sum_l \frac{jw\mu}{k_d^2-k_{lu}^2}\frac{\langle J_f, E_{r,lu}\rangle^2}{\|E_{r,lu}\|^2} \tag{38}$$

Z_{in} shown above already includes the effects of dielectric losses, as $k_d^2 = w^2\mu\,\varepsilon_d = w^2\mu\,\varepsilon_r\varepsilon_o(1-j\tan\delta_d)$. Additionally, the conductor and radiation losses can be taken into account by substituting $\tan\delta_d$ by an effective loss tangent ($\tan\delta_{eff}$) that includes all losses in the dielectric ($\tan\delta_d$), in the conductor ($\tan\delta_c$), and also radiation losses ($\tan\delta_r$), i.e.:

$$\tan\delta_{eff} = \tan\delta_d + \tan\delta_c + \tan\delta_r \tag{39}$$

The loss tangent due to conductor loss is given by [14]:

$$\tan\delta_c = \frac{P_c}{w(W_e+W_m)} \tag{40}$$

where P_c is the power loss in the conductor, and W_e and W_m are the average electric and magnetic energy stored in the cavity region, calculated at the resonance frequency of each mode (where $W_e = W_m$), and given by:

$$P_{c,lu} = \frac{R_s}{2}\iint_S |\bar{H}_{lu}|^2\,ds \tag{41}$$

$$W_{e,lu} = \frac{1}{4}\varepsilon_o\varepsilon_r\iiint_V |\bar{E}_{lu}|^2\,dv \tag{42}$$

where R_s is the surface resistance of the conductor, S is the internal cavity surface, V is the cavity volume, and the components of electrical and magnetic fields of lu mode are given by (4), (7) and (8). Similarly the loss tangent due to radiation is given by:

$$\tan\delta_r = \frac{P_r}{w(W_e+W_m)} \tag{43}$$

where P_r is the power loss due to radiation, obtained at the mode resonance. It can be obtained from the coefficients of the external modes (35) and (36) and their radiating powers (29) and (30) when the equivalent magnetic currents in (35) and (36) are due only to cavity mode lu:

$$P_{r,lu} = \sum_{n=1}^{\infty}\sum_{m=-n}^{n}\left[|e_{nm}|^2\,P_{r,mn}^{TM} + |f_{nm}|^2\,P_{r,mn}^{TE}\right] \tag{44}$$

Substituting $\tan\delta_d$ by $\tan\delta_{eff}$ in (38):

$$Z_{in} = -\frac{h}{I_o^2}\sum_u\sum_l \frac{jw\mu}{k_{eff}^2-k_{lu}^2}\frac{\langle J_f, E_{r,lu}\rangle^2}{\|E_{r,lu}\|^2} \tag{45}$$

where $k_{eff}^2 = w^2\mu\,\varepsilon_r\varepsilon_o(1-j\tan\delta_{eff})$.

4. Application of method of moments

We will now briefly discuss the application of MoM to the same geometry presented in Fig. 1. Detailed description can be found in [27]. The spherical patches are also fed as shown in Fig. 2. As mentioned earlier the MoM seeks to determine the distribution of electric currents on the patches that satisfies the boundary condition [18]. And the radiation properties follow from the current distribution [36].

Let the surface electrical current on the patches be expanded into a set of functions, known as basis functions, as follows:

$$J_\theta(\theta) = \sum_{q=1}^{Q_\theta} a_q J_{\theta q}(\theta) \tag{46}$$

$$J_\phi(\phi) = \sum_{p=1}^{P_\phi} b_p J_{\phi p}(\phi) \tag{47}$$

where a_q and b_p are the expansion coefficients that will be determined using MoM. The basis functions are given by

$$J_{\theta q}(\theta) = \frac{\sin\left(\frac{q\pi}{\Delta\theta}(\theta-\theta_1)\right)}{\sin\theta} \tag{48}$$

$$J_{\phi p}(\phi) = \sin\left(\frac{p\pi}{\Delta\phi}(\phi-\phi_1)\right) \tag{49}$$

where $\Delta\theta = \theta_2-\theta_1$. These basis functions present a sinusoidal variation across the patch.

The tangential components of the electric field in spectral domain are related to the surface electric current on the patches through the dyadic Green's functions [27]:

$$\tilde{E}_t^o(r,n,m) = \overline{\overline{G_t^{Eo}}}(r,n)\tilde{J}(n,m) \tag{50}$$

$$\tilde{E}_t^d(r,n,m) = \overline{\overline{G_t^{Ed}}}(r,n)\tilde{J}(n,m) \tag{51}$$

The surface current distribution on the patches are determined from imposing the boundary condition of zero tangential component of electric field on the patch surface. The MoM will transform the resulting integral equations into a linear system where the unknowns are the coefficients (a_q and b_p) of the surface electrical currents. The boundary conditions on the patches are:

$$E_\theta(J_\theta) + E_\theta(J_\phi) + E_\theta(J_f) = 0 \tag{52}$$

$$E_\phi(J_\theta) + E_\phi(J_\phi) + E_\phi(J_f) = 0 \tag{53}$$

Expanding the surface electrical currents on the patch as in (46)–(47) leads to:

$$\sum_{q=1}^{Q_\theta} a_q E_\theta(J_{\theta q}) + \sum_{p=1}^{P_\phi} b_p E_\theta(J_{\phi p}) = -E_\theta(J_f) \tag{54}$$

$$\sum_{q=1}^{Q_\theta} a_q E_\phi(J_{\theta q}) + \sum_{p=1}^{P_\phi} b_p E_\phi(J_{\phi p}) = -E_\phi(J_f) \tag{55}$$

Defining the symmetric product:

$$\langle f,g\rangle_s = \int_0^\pi\int_{-\pi}^{\pi} f(\theta,\phi)g(\theta,\phi)r_2^2\sin\theta\,d\phi\,d\theta \tag{56}$$

and taking these products of (54) and (55) by a set of testing functions, which are chosen the same as the basis functions, results in a Galerkin method. The resulting linear system ($[Z][I] = [V]$) can be written as [27]:

$$\begin{bmatrix}[Z^{\theta\theta}] & [Z^{\theta\phi}]\\ [Z^{\phi\theta}] & [Z^{\phi\phi}]\end{bmatrix}\begin{bmatrix}[a]\\ [b]\end{bmatrix} = \begin{bmatrix}[V^\theta]\\ [V^\phi]\end{bmatrix} \tag{57}$$

where the elements of matrix [Z] are of the following form:

$$Z_{test,basis} = \langle \bar{E}(\bar{J}_{basis}), \bar{J}_{test}\rangle_s = r_2^2\sum_{m=-\infty}^{\infty}\sum_{n=|m|}^{\infty}\left[\tilde{J}_{test}(n,-m)\right]^t\overline{\overline{G_t^{Eo}}}(r_2,n) \times\left[\tilde{J}_{basis}(n,m)\right] \tag{58}$$

where $test$ and $basis$ refer to either θ or ϕ. In (57) [a] and [b] are column matrices with the unknown coefficients. The elements of the matrix [V], with the aid of reciprocity theorem, can be obtained from:

$$V_{test} = -\langle\bar{E}(J_f), \bar{J}_{test}\rangle_s = -\frac{r_2}{jw\varepsilon_d}\sum_{m=-\infty}^{\infty}\sum_{n=|m|}^{\infty}\frac{\sqrt{S(n)}\,J_u(n,m)}{D_1(n,r_1,r_2)}\times \left(\frac{\eta_d}{\eta_o}\frac{\hat{H}_n^{(2)}(k_or_2)}{\hat{H}_n^{(2)\prime}(k_or_2)} - \frac{D_3(n,r_1,r_2)}{D_1(n,r_1,r_2)}\right)^{-1}\int_{r_1}^{r_2} D_3(n,r_1,r)\times\bar{J}_f(r,n,-m)dr \tag{59}$$

The coefficients of the currents on the patches, a_q and b_p, are obtained from solving the MoM linear system.

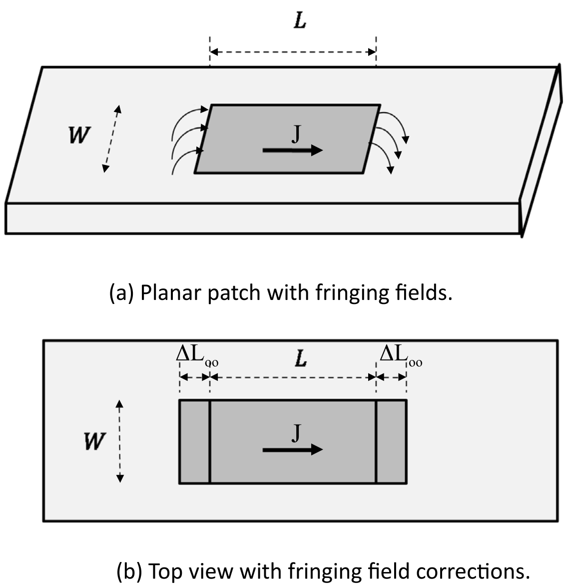

Fig. 3. (a) Planar patch with fringing fields. (b) Top view with fringing field corrections.

The input impedance is given by the variational expression [36]:

$$Z_{in} = -\frac{1}{I_o^2} \iint_S \bar{E}(\bar{J}) \cdot \bar{J}_f \, ds \tag{60}$$

Expanding the surface current distribution on the patch $\bar{J}$ in basis functions, and using (59) together with reciprocity theorem, results:

$$Z_{in} = \frac{1}{I_o^2} \left[\sum_{q=1}^{Q_\theta} a_q V_q^\theta + \sum_{p=1}^{P_\phi} b_p V_p^\phi \right] \tag{61}$$

5. Fringing field correction

Despite the simplicity of the formulation, the cavity method presents accurate results for radiation pattern, as it will be shown in Section 6. The biggest limitation results from considering that the fields in the dielectric layer exist only below the patch, while in fact the fields extend beyond the patch limits, as shown in Fig. 3a for a planar microstrip antenna. This supposition results in inaccurate resonance frequency. To compensate for this drawback a correction of the dimensions of the planar patch is used for simulation purposes, including fringing field corrections (or extensions) ΔL_∞. The cavity method is now applied as if the patch had dimension $L+2\Delta L_\infty$, and the fields were concentrated below it, as shown in Fig. 3b. A possible correction proposed in [37] is used for planar microstrip patch of resonant length L and width W.

$$\Delta L_\infty = 0.412\, h \, \frac{\left(\varepsilon_{eff} + 0.3\right)\left(W/h + 0.264\right)}{\left(\varepsilon_{eff} - 0.258\right)\left(W/h + 0.8\right)} \tag{62}$$

where ε_{eff} stands for an effective dielectric constant given by:

$$\varepsilon_{eff} = \frac{\varepsilon_r + 1}{2} + \frac{(\varepsilon_r - 1)}{2\sqrt{1 + 10\, h/W}} \tag{63}$$

The planar correction ΔL_∞ shown above has taken into account the effects of the dielectric thickness (h), dielectric constant (ε_r), and the width of the patch (W). Unfortunately ΔL_∞ is not a good approximation for fringing fields of spherical microstrip patches, and the resonance frequency of spherical patches obtained from cavity method with planar correction ΔL_∞ is usually shifted from measurement data or results from more accurate methods.

This section describes how the planar correction ΔL_∞ can be modified to take into account the curvature of the spherical patch. Results from method of moments procedure presented in Section 4 will be treated as references, as it is a full-wave solution already validated [27]. Therefore we should seek for an spherical correction (ΔL_r) such that the application of cavity method (Section 3) will result in the same resonance frequencies provided by the method of moments. It should also be understood that the curvature effects on fringing fields are different for different dielectric constants.

In the following procedure L is the resonant length of the spherical–rectangular microstrip antenna, which can be either in θ or ϕ directions. Application of cavity method with planar fringing field correction leads to a resonance frequency $f_{cav}(r_2, \varepsilon_r)$ for a resonance length of $(L + 2\,\Delta L_\infty) = \lambda_{cav}/2$, where λ_{cav} is the wavelength at f_{cav}. Therefore the phase velocity values $v_p = f_{cav}\, \lambda_{cav} = f_{cav}\, 2(L + 2\,\Delta L_\infty)$. It is wanted to determine the right spherical correction ΔL_r such that application of cavity method for a length $(L + 2\,\Delta L_r)$ would result in the correct resonance frequency $f_{MoM}(r_2, \varepsilon_r)$, as the method of moments is been used as a reference. Assuming that the antenna will present the same effective dielectric constant with either fringing field corrections, $v_p = f_{MoM}\, 2(L + 2\,\Delta L_r)$. Therefore ΔL_r should be such that:

$$\left(L + 2\,\Delta L_r\right)\, f_{MoM}(r_2, \varepsilon_r) = \left(L + 2\,\Delta L_\infty\right)\, f_{cav}(r_2, \varepsilon_r) \tag{64}$$

Therefore:

$$\Delta L_r = \frac{1}{2}\left[\frac{f_{cav}(r_2, \varepsilon_r)}{f_{MoM}(r_2, \varepsilon_r)}\, \left(L + 2\,\Delta L_\infty\right) - L\right] \tag{65}$$

The spherical fringing field correction ΔL_r shown above is valid only for the first TM mode (first resonance in the given direction), as the field distribution changes for different modes, leading to different fringing field effects. The spherical correction ΔL_r could be easily obtained if the function f_{cav}/f_{MoM} were readily available for any given radius r_2 and any dielectric constant ε_r. A simple model for f_{cav}/f_{MoM} is obtained in the least squares sense as follows:

1. The function f_{cav}/f_{MoM} is modeled as:
$$\frac{f_{cav}(r_2, \varepsilon_r)}{f_{MoM}(r_2, \varepsilon_r)} = A(\varepsilon_r)\frac{r_2}{L} + B(\varepsilon_r) + C(\varepsilon_r)\frac{L}{r_2} \tag{66}$$
where
$$A(\varepsilon_r) = a_1 + \frac{a_2}{\varepsilon_r} \tag{67}$$
$$B(\varepsilon_r) = b_1 + \frac{b_2}{\varepsilon_r} \tag{68}$$
$$C(\varepsilon_r) = c_1 + \frac{c_2}{\varepsilon_r} \tag{69}$$
2. The values of f_{MoM} and f_{cav} are obtained for several values of radius r_2 and dielectric constant (ε_r) using method of moments (Section 4) and cavity method (Section 3) using planar correction ΔL_∞, respectively. The values of the radius r_2 ranged from $\lambda_d/5$ to $2\,\lambda_d$, where λ_d is the dielectric wavelength. And the dielectric constant ranged from 1 to 10.
3. For each combination of r_2 and ε_r (66) represents a line of a linear system with unknowns a_1, a_2, b_1, b_2, c_1, and c_2:
$$\frac{r_2}{L}a_1 + \frac{r_2}{\varepsilon_r L}a_2 + b_1 + \frac{1}{\varepsilon_r}b_2 + \frac{L}{r_2}c_1 + \frac{L}{\varepsilon_r r_2}c_2 = \frac{f_{cav}(r_2, \varepsilon_r)}{f_{MoM}(r_2, \varepsilon_r)} \tag{70}$$
4. As there are many more lines (combinations of r_2 and ε_r) than unknowns, the linear system is overdetermined, and solved in the least squares sense, resulting in:
$$A(\varepsilon_r) = 0.00357 - \frac{0.00089}{\varepsilon_r} \tag{71}$$
$$B(\varepsilon_r) = 0.9695 + \frac{0.0450}{\varepsilon_r} \tag{72}$$
$$C(\varepsilon_r) = 0.0081 + \frac{0.0067}{\varepsilon_r} \tag{73}$$

Therefore the spherical fringing field correction ΔL_r is given by (65) where f_{cav}/f_{MoM} is given by (66), with coefficients $A(\varepsilon_r)$, $B(\varepsilon_r)$, and $C(\varepsilon_r)$ given by (71)–(73), and planar fringing field correction ΔL_∞ given by (62).

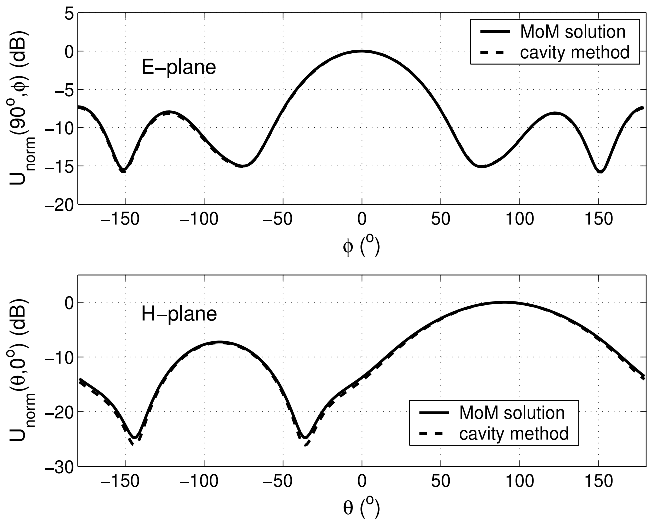

Fig. 4. Normalized radiation patterns of a spherical–rectangular patch at E-plane (xy plane) and H-plane ($\phi = 0°$ plane). $\theta_c = 90°$, $\phi_c = 0°$, $r_1 = 18.5$ cm, $h = 4.5$ mm, $\varepsilon_r = 1$, $W_\theta = W_\phi = 20$ cm, $d_\theta = 0$, $d_\phi = 8$ cm, and $W_f = 6.5$ mm.

6. Results and comments

Consider the spherical–rectangular patch, as shown in Fig. 1. A spherical conductor of radius $r_1 = 18.5$ cm is covered by a layer of foam ($\varepsilon_r = 1$) of thickness $h = 4.5$ mm. A patch of width $W_\theta = 20$ cm in θ-direction, and $W_\phi = 20$ cm in ϕ-direction, is centered at $\theta_c = 90°$ and $\phi_c = 0°$. The patch is fed at $\theta_f = 90°$, at a point $d_\phi = 8$ cm from the patch center, and the probe is modeled as a strip of width $W_f = 6.5$ mm. As a result the patch is ϕ-polarized. Fig. 4 shows the normalized radiation patterns using the cavity method and MoM. Fig. 4a shows the radiation in E-plane (xy plane), as a function of angle ϕ. It can be observed a maximum radiation in the direction of the antenna center, and that both methods present almost indistinguishable results. Fig. 4b shows the radiation pattern in the H-plane ($\phi = 0°$ plane), as a function of θ. Again the results for both methods are very close, and the maximum radiation happens in front of the antenna ($\theta = 90°$). It can also be observed a backlobe with maximum at $\theta = -90°$, which means the opposite direction to the maximum radiation.

Figs. 5 and 6 show the input impedance (resistance and reactance) of the same spherical–rectangular patch. Results presented are from application of method of moments, from measurements [25], and from application of cavity method with planar fringing field corrections (ΔL_∞). An excellent agreement can be observed between the results from method of moments and the measurements, with a small frequency shift at resonance. On the other hand it can be observed that the application of cavity method with planar correction does not take into account the fringing fields accurately, as the resonance frequency is significantly apart from previous results.

In order to correct the resonance frequency of the patch predicted by cavity method, the planar fringing field correction (ΔL_∞) is now substituted by the spherical one (ΔL_r). The new results of cavity method with spherical correction are compared to those from method of moments in Fig. 7. It can be observed that the use of spherical correction has brought the resonance frequency of cavity method very close to results from MoM. This shows that, despite its simplicity, the cavity method with the aid of the spherical correction is able to provide accurate results for spherical microstrip patches, taking into account the fringing fields.

Additional examples are presented in Figs. 8 and 9, comparing results using method of moments and those using cavity method with spherical correction. Fig. 8 presents the results for a new dielectric constant equal to 2.2. Fig. 9 presents the results for two different radii

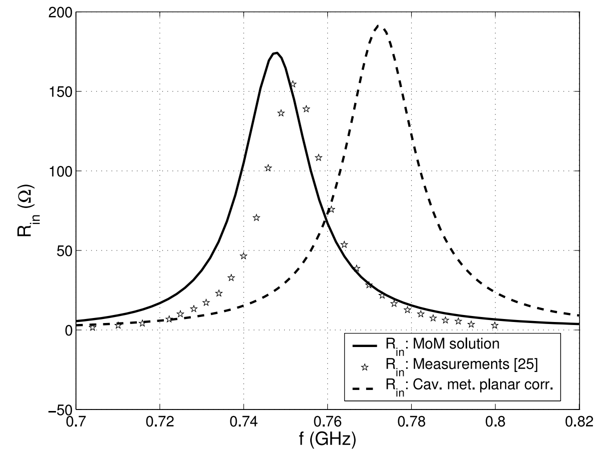

Fig. 5. Input Resistance of a spherical–rectangular patch. $\theta_c = 90°$, $\phi_c = 0°$, $r_1 = 18.5$ cm, $h = 4.5$ mm, $\varepsilon_r = 1$, $W_\theta = W_\phi = 20$ cm, $d_\theta = 0$, $d_\phi = 8$ cm, and $W_f = 6.5$ mm.

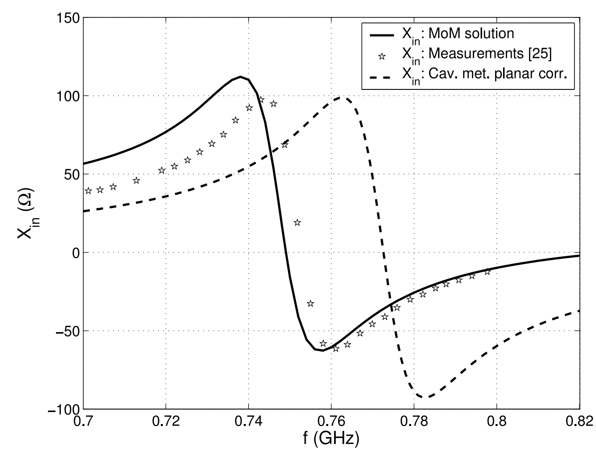

Fig. 6. Input Reactance of a spherical–rectangular patch. $\theta_c = 90°$, $\phi_c = 0°$, $r_1 = 18.5$ cm, $h = 4.5$ mm, $\varepsilon_r = 1$, $W_\theta = W_\phi = 20$ cm, $d_\theta = 0$, $d_\phi = 8$ cm, and $W_f = 6.5$ mm.

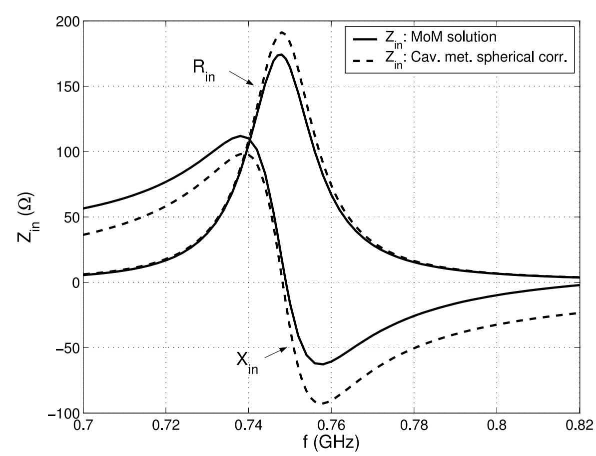

Fig. 7. Input Impedance of a spherical–rectangular patch. $\theta_c = 90°$, $\phi_c = 0°$, $r_1 = 18.5$ cm, $h = 4.5$ mm, $\varepsilon_r = 1$, $W_\theta = W_\phi = 20$ cm, $d_\theta = 0$, $d_\phi = 8$ cm, and $W_f = 6.5$ mm.

of the sphere. In both cases the cavity method with spherical correction led to accurate results.

The spherical fringing field correction ΔL_r, given by (65), takes into account variations of the dielectric thickness h through the planar correction ΔL_∞ (62), but it was not part of the least square optimization.

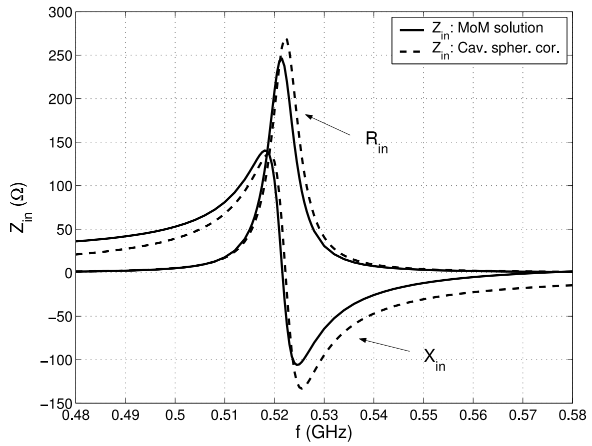

Fig. 8. Input Impedance of a spherical–rectangular patch with $\epsilon_r = 2.2$, $\theta_c = 90°$, $\phi_c = 0°$, $r_1 = 18.5$ cm, $h = 4.5$ mm, $W_\theta = W_\phi = 20$ cm, $d_\theta = 0$, $d_\phi = 8$ cm, and $W_f = 6.5$ mm.

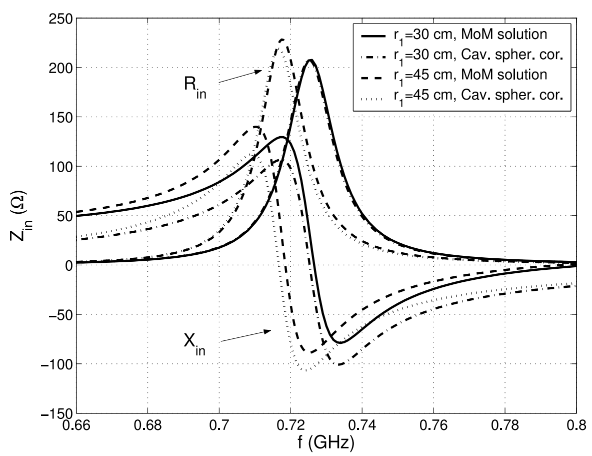

Fig. 9. Input Impedance of a spherical–rectangular patch with $r_1 = 30$ cm and $r_1 = 45$ cm, $\theta_c = 90°$, $\phi_c = 0°$, $h = 4.5$ mm, $\epsilon_r = 1$, $W_\theta = W_\phi = 20$ cm, $d_\theta = 0$, $d_\phi = 8$ cm, and $W_f = 6.5$ mm.

In order to evaluate results for different dielectric thickness Fig. 10 shows a comparison of input impedance using method of moments, cavity method with planar correction, and cavity method with spherical correction, for $h = 3$ mm, keeping $r_2 = 189.5$ mm. It can be observed that the use spherical correction led to more accurate results when compared to those using planar correction. In this case the shift of resonance frequency when using spherical correction is equal to 6 MHz. For different dielectric thicknesses a shift of resonance frequency of about 10 MHz should be expected.

Some final comments on the computational resources demanded by the cavity method and MoM. MoM does not require as much memory as differential methods, like Finite Element Method. But when compared to cavity method, it does require more space for storing the linear system, as well as to store results of some integrals that happen many times. Comparing the computational time, it was observed that MoM took over 100 times more time than cavity method, which needed a fraction of a second per frequency point.

7. Conclusions

This paper presented a new approximate model for fringing field correction for spherical–rectangular microstrip antennas. The patch was analyzed using both cavity method and method of moments. It was shown that both methods are equivalent regarding the radiation

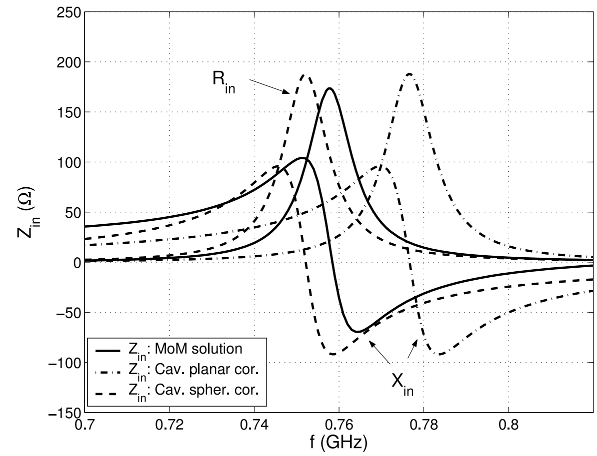

Fig. 10. Input Impedance of a spherical–rectangular patch with $h = 3$ mm, $\theta_c = 90°$, $\phi_c = 0°$, $r_1 = 18.65$ cm, $\epsilon_r = 1$, $W_\theta = W_\phi = 20$ cm, $d_\theta = 0$, $d_\phi = 8$ cm, and $W_f = 6.5$ mm.

diagrams. And that the use of spherical fringing field correction can make cavity method results to be comparable to those from method of moments, in a fraction of the computational time required.

Declaration of competing interest

The authors declare that they have no known competing financial interests or personal relationships that could have appeared to influence the work reported in this paper.

Appendix. Normalized vector Legendre series

A normalized vector Legendre series of a two-dimensional field $\bar{J}(\theta,\phi)$ is given by [15,22]:

$$\bar{J}(\theta,\phi) = \begin{bmatrix} J_\theta(\theta,\phi) \\ J_\phi(\theta,\phi) \end{bmatrix} = \sum_{m=-\infty}^{\infty} \sum_{n=|m|}^{\infty} \frac{1}{\sqrt{S(n)}} \overline{\overline{L}}(n,m,\theta)\tilde{J}(n,m)e^{jm\phi} \tag{74}$$

where

$$\tilde{J}(n,m) = \begin{bmatrix} J_u(n,m) \\ J_d(n,m) \end{bmatrix} = \frac{1}{\sqrt{S(n)}} \int_0^\pi \int_{-\pi}^{\pi} \overline{\overline{L}}(n,m,\theta)\bar{J}(\theta,\phi)\, e^{-jm\phi} \sin\theta \, d\theta \, d\phi \tag{75}$$

and

$$\overline{\overline{L}}(n,m,\theta) = \begin{bmatrix} \frac{\partial}{\partial\theta}\bar{P}_n^{|m|}(\cos\theta) & -jm\frac{\bar{P}_n^{|m|}(\cos\theta)}{\sin\theta} \\ jm\frac{\bar{P}_n^{|m|}(\cos\theta)}{\sin\theta} & \frac{\partial}{\partial\theta}\bar{P}_n^{|m|}(\cos\theta) \end{bmatrix} \tag{76}$$

$$S(n) = 4\pi\frac{n(n+1)}{2n+1} \tag{77}$$

The normalized associated Legendre functions $\bar{P}_n^m(.)$ relates to the associated Legendre functions $P_n^m(.)$ by:

$$\bar{P}_n^m(\cos\theta) = \sqrt{\frac{(n-m)!}{(n+m)!}}P_n^m(\cos\theta) \tag{78}$$

References

[1] Bekri Y, Benabdallah N, Lachachi D, Benahmed N. Expressions for the TEM-parameters deduced from FEM-analyses for shielded and coupled cylindrical striplines. AEU - Int J Electron Commun 2016;70:241–9. http://dx.doi.org/10.1016/j.aeue.2015.11.006.

[2] Jarboua I, Ammar N, Aguili T, Baudr H. Radiation pattern and scattering parameter for multilayer cylindrical loop antenna using the iterative method WCIP. AEU - Int J Electron Commun 2019;101:192–9. http://dx.doi.org/10.1016/j.aeue.2019.01.024.

[3] Hosseinbeig A, Kamyab M, Meiguni JS. Theory of aperture-coupled hemispherical dielectric resonator antennas with radiating elements. AEU - Int J Electron Commun 2013;67:975–80. http://dx.doi.org/10.1016/j.aeue.2013.05.010.

[4] Mukherjee B, Kumar VD, Gupta M. A novel Hemispherical Dielectric Resonator Antenna on an Electromagnetic Band Gap substrate for broadband and high gain systems. AEU - Int J Electron Commun 2014;68:1185–90. http://dx.doi.org/10.1016/j.aeue.2014.06.007.

[5] Jafargholi A, Kamyab M. Input impedance analysis of dielectric covered/loaded biconical antennas using mode-matching theory. AEU - Int J Electron Commun 2012;66:828–32. http://dx.doi.org/10.1016/j.aeue.2012.02.001.

[6] Jovicevic S, Jovanovic A. The analysis of the Biconical Antenna by the Least-Squares Boundary Residual Method. AEU - Int J Electron Commun 2003;57:415–9. http://dx.doi.org/10.1078/1434-8411-54100194.

[7] Wong KL. Design of nonplanar microstrip antennas and transmission lines. John Wiley & Sons; 1999, http://dx.doi.org/10.1002/0471200662.

[8] Josefsson L, Persson P. Conformal array antenna theory and design. Wiley-Interscience; 2006, http://dx.doi.org/10.1002/047178012X.

[9] Krowne C. Radiation efficiency for spherical-rectangular microstrip antenna. In: IEEE AP-S international symposium. 1982, p. 171–4. http://dx.doi.org/10.1109/APS.1982.1148878.

[10] Wu K, Kauffman J. Radiation Pattern Computations for Spherical-Rectangular Microstrip Antennas. In: IEEE antennas propagat. int. symposium. 1983, p. 43–6. http://dx.doi.org/10.1109/APS.1983.1149120.

[11] Luk KM, Tam W. Patch antennas on a Spherical Body. IEE Proc-H 1991;138:103–8. http://dx.doi.org/10.1049/ip-h-2.1991.0017.

[12] Das A, Das SK, Narasimhan MS. Radiation characteristics of Wraparound Microstrip Antenna on Spherical Body. IEEE Trans Antennas and Propagation 1991;39:1031–4. http://dx.doi.org/10.1109/8.86925.

[13] Lima ACC, Descardeci JR, Giarola AJ. Microstrip antenna on a spherical surface. In: IEEE AP-S digest. 1991, p. 820–3. http://dx.doi.org/10.1109/APS.1991.174970.

[14] Ferreira DB, Lacava JCS. Microstrip Antennas Conformed onto Spherical Surfaces. In: Nasimuddin N, editor. Microstrip antennas. Intech; 2011, p. 83–108. http://dx.doi.org/10.5772/15678.

[15] Tam WY, Luk KM. Far field analysis of spherical-circular microstrip antennas by electric surface current models. IEE Proc-H 1991;138:98–102. http://dx.doi.org/10.1049/ip-h-2.1991.0016.

[16] Ke B, Kishk AA. Analysis of spherical circular microstrip antennas. IEE Proc-H 1991;138:542–8. http://dx.doi.org/10.1049/ip-h-2.1991.0091.

[17] Kishk AA. Analysis of Spherical Annular Microstrip Antennas. IEEE Trans Antennas and Propagation 1993;41:338–43. http://dx.doi.org/10.1109/8.233129.

[18] Harrington RF. Field computation by moment method. Wiley-IEEE Press; 1993, http://dx.doi.org/10.1109/9780470544631.

[19] Tam WY, Luk KM. Resonance in spherical-circular microstrip structures. IEEE Trans Microw Theory Tech 1991;39:700–4. http://dx.doi.org/10.1109/22.76435.

[20] Wong KL, Hsiao SF, Chen HT. Resonance and radiation of a superstrateloaded spherical-circular microstrip patch antenna. IEEE Trans Antennas and Propagation 1993;41:686–90. http://dx.doi.org/10.1109/8.222290.

[21] Tam WY, Lai AKY, Luk KM. Input impedance of spherical microstrip antenna. IEE Proc Microw Antennas Propag 1995;142:285–8. http://dx.doi.org/10.1049/ip-map:19951931.

[22] Sipus Z, Burum N, Bartolic J. Analysis of Rectangular Microstrip Patch Antennas on Spherical Structures. Microw Opt Technol Lett 2003;36:276–80. http://dx.doi.org/10.1002/mop.10741.

[23] Burum N, Sipus Z, Bartolic J. Mutual coupling between Spherical-Rectangular Microstrip Antennas. Microw Opt Technol Lett 2004;40:387–91. http://dx.doi.org/10.1002/mop.11389.

[24] Giang TVB. A systematic approach to the analysis of spherical multilayer structures and its applications (thesis), Technical University of Hamburg-Harburg; 2005.

[25] Sipus Z, Burum N, Skokic S, Kildal PS. Analysis of Spherical arrays of Microstrip Antennas using Moment Method in Spectral Domain. IEE Proc Microw Antennas Propag 2006;153:533–43. http://dx.doi.org/10.1049/ip-map:20050262.

[26] Costa LA, Pereira-Filho OMC, Moreira FJS. Input impedance of Rectangular Microstrip Antennas on Spherical Bodies using MoM and Attachment Modes. In: IEEE AP-S digest. 2006, p. 3947–50. http://dx.doi.org/10.1109/APS.2006.1711489.

[27] Costa LA, Pereira-Filho OMC, Moreira FJS. Quasi-trapezoidal Microstrip Spherical Patches and Arrays. IET Microw Antennas Propag 2016;10:53–60. http://dx.doi.org/10.1049/iet-map.2015.0145.

[28] Sipus Z, Kildal PS, Leijon R, Johansson M. An algorithm for Calculating Greens Functions for Planar, Circular Cylindrical and Spherical multilayer Substrates. Appl Comput Electromagn Soc J 1998;13:243–54.

[29] Okhmatovski VI, Cangellaris AC. Efficient calculation of the Electromagnetic Dyadic Green's function in Spherical Layered Media. IEEE Trans Antennas and Propagation 2003;51:3209–20. http://dx.doi.org/10.1109/TAP.2003.820952.

[30] Khamas SK. A generalized asymptotic Extraction Solution for Antennas in Multilayered Spherical Media. IEEE Trans Antennas and Propagation 2010;58:3743–7. http://dx.doi.org/10.1109/TAP.2010.2071371.

[31] Giang TVB, Dreher A. Analysis method of Microstrip Antennas on Hemispherical Multilayer Structures. IEEE Trans Antennas Propag 2008;56:3324–7. http://dx.doi.org/10.1109/TAP.2008.929544.

[32] Tsitsas NL, Valagiannopoulos CA. Mathematical Modeling of Spherical Microstrip Antennas and Applications. In: Nasimuddin N, editor. Microstrip antennas. Intech; 2011, p. 109–30. http://dx.doi.org/10.5772/15467.

[33] Khamas SK. Electromagnetic radiation by Antennas of Arbitrary shape in a Layered Spherical Media. IEEE Trans Antennas and Propagation 2009;57:3827–34. http://dx.doi.org/10.1109/TAP.2009.2033444.

[34] Meiguni JS, Kamyab M, Hosseinbeig A. Theory and experiment of Spherical Aperture-Coupled Antennas. IEEE Trans Antennas and Propagation 2013;61:2397–403. http://dx.doi.org/10.1109/TAP.2013.2244836.

[35] Richards WF, Lo YT, Harrison DD. An improved theory for microstrip antennas and applications. IEEE Trans Antennas Propag 1981;29:38–46. http://dx.doi.org/10.1109/TAP.1981.1142524.

[36] Harrington RF. Time-Harmonic electromagnetic fields. Wiley-IEEE Press; 2001, http://dx.doi.org/10.1109/9780470546710.

[37] Hammerstad EO. Equations for microstrip circuit design. In: Proc. 5th European micro. conf.. 1975, p. 268–72. http://dx.doi.org/10.1109/APS.1979.1148165.